

Surface aging at olivine LiFePO₄: a direct visual observation of iron dissolution and the protection role of nano-carbon coating

Cite this: *J. Mater. Chem. A*, 2013, **1**, 1579

Jiajun Wang,^a Jinli Yang,^a Yongji Tang,^a Ruying Li,^a Guoxian Liang,^b Tsun-Kong Sham^c and Xueliang Sun^{*a}

LiFePO₄ has attracted much attention as a potential cathode material for advanced lithium-ion batteries due to its superior thermal stability. In spite of this, LiFePO₄ still suffers from fast capacity fading at high temperature and/or moisture-contaminated electrolyte. The influence of moisture and the detailed corrosion mechanism is still not clear. Here, for the first time, we present a direct visual observation of the surface corrosion process at olivine LiFePO₄ stored in moisture-contaminated electrolyte, and found the direct relationship between iron dissolution and LiFePO₄ corrosion. By using the LiFePO₄ ingot sample with a flat surface as model materials, iron dissolution and surface chemistry change can be clearly observed and identified by field-emission scanning electron microscopy (SEM), time-of-flight-secondary ion mass spectroscopy (TOF-SIMS), and X-ray absorption near-edge structure (XANES). These iron dissolutions at some corrosion sites evoked the overall LiFePO₄ surface corrosion. A significant improvement of the surface stability of LiFePO₄ was obtained by nano-carbon coating, and the carbon surface layer protects LiFePO₄ from direct contact with corrosive medium, effectively restraining the surface corrosion and preserving the initial surface chemistry of LiFePO₄.

Received 1st October 2012

Accepted 9th November 2012

DOI: 10.1039/c2ta00521b

www.rsc.org/MaterialsA

Introduction

Olivine LiFePO₄ has been subjected to numerous studies as a cathode material for lithium-ion batteries (LIBs) since it was first reported by Padhi *et al.*¹ Its high structural stability and superior cycle performance make it a highly safe cathode material for advanced LIBs applied in electric vehicles. Some conventional oxide cathodes such as LiCoO₂ can release O₂ during the cycle process especially at elevated temperatures.^{2–4} The released O₂ may ignite the organic solvents in electrolyte and result in fire and even explosion. The olivine-type LiFePO₄ has strong covalent P–O bonds in the (PO₄)^{3–} polyanion, which stabilize oxygen and inhibit O₂ release at high states of charging, thus making them excellent stable and safe cathode materials.^{1,5,6}

In general, LiFePO₄ is believed to be chemically inert upon immersion in electrolytes. Nevertheless, despite excellent long-term cycle stability at low temperature, LiFePO₄ still suffers from fast capacity fading at high temperature and/or moisture-contaminated electrolyte.^{7–11} The accelerated capacity loss was generally attributed to iron dissolution from LiFePO₄ attacked

by acid species such as HF in moisture-contaminated LiPF₆ electrolyte.^{12–14} Nazar's group investigated the stability of the LiFePO₄ olivine cathode under various electrolyte solutions, and found the presence of iron dissolution through ICP analysis, especially in H₂O contaminated LiPF₆ electrolyte at evaluated temperature.¹⁵ Similar iron dissolution phenomena were also reported at room temperature condition.¹¹ The iron dissolution destroys the LiFePO₄ structure and decreases the active material's capacity. Further, these dissolved iron ions may move to the anode electrode and result in continuous formation of solid electrolyte interphase (SEI) due to the good catalytic effect of iron.^{16–18} The formation of this thick SEI layer consumes a lot of lithium ions, leading to more capacity loss.

Although iron dissolution has been demonstrated to be one of the major sources for the capacity loss of LiFePO₄, understanding and monitoring the iron dissolution evolution is still scarce.^{19,20} The novelty of this work is to present a direct observation of the iron dissolution process at LiFePO₄ and provide key evidence of the protective role of the carbon nano-coating layer. By aging a model material (LiFePO₄ ingot sample) under moisture-contaminated electrolyte which is closer to the practical application conditions, combining with various material characterization tools, iron dissolution evolution was directly observed and identified. The possible aging mechanism with iron dissolution was also proposed. Moreover, we highlight here that a significant improvement of the surface stability of LiFePO₄ was obtained by a protective carbon nanolayer. The

^aDepartment of Mechanical and Materials Engineering, University of Western Ontario, London, Ontario, N6A 5B9, Canada. E-mail: xsun@eng.uwo.ca

^bPhostech Lithium Inc., 1475 Rue Marie-Victorin, St-Bruno, QC, J3V 6B7, Canada

^cDepartment of Chemistry, University of Western Ontario, London, Ontario, N6A 5B7, Canada

understanding and methodology here could be also extended to other olivine phosphates (e.g. LiMnPO_4 , LiFeMnPO_4), more promising next-generation cathode materials.

Experimental

The ingot sample was prepared by a melt casting process recently developed in Phostech Lithium Inc.^{21,22} To get a flat surface for better observation and study, the melt sample was cut into small size (cm), and then was polished by various Aluminum Oxide sandpapers from coarse (Grit 120) to fine grades (Grit 1500). After ultrasonic cleaning in ethanol several times, a LiFePO_4 ingot sample with a clean and flat surface was thus obtained.

Carbon coating experiments were carried out on polished LiFePO_4 with a spray pyrolysis system, which was similar to the synthesis of other nanomaterials.^{23,24} Ethanol was used as the carbon source and argon was used as the carrying and protecting gas. Briefly, the ingot sample with the flat surface was put in a quartz tube and Ar was introduced into the quartz tube for 20 min to eliminate the air. Subsequently the furnace was heated to 650 °C and the carbon coating process was performed for 20 min. After carbon coating, the coated sample was cooled to room temperature within the furnace still under the protection of Ar atmosphere.

The aging experiment was performed by simply soaking the samples in water-contaminated (400 ppm) 1 M LiPF_6 in EC/DMC electrolyte for various durations: 8 h, 16 h, 24 h and 32 h, at ambient temperature. After the aging process, the samples

were rinsed, ultrasonically cleaned, and dried under ambient condition for 1 day. The resulting samples were ready for further characterization.

Focused ion beam lithography was performed on LEO (Zeiss) 1540XB FIB/SEM, and subsequently the slices were plucked by the nanomanipulator. After the tip of the end effector was folded over and removed from the nanomanipulator rod, the sample can be mounted in a HRTEM sample holder.

The morphology and microstructure of the samples were characterized by a Hitachi S-4800 field-emission scanning electron microscope (SEM). To confirm the surface chemistry change after the aging process, the aged LiFePO_4 materials were examined using a time-of-flight-secondary ion mass spectroscopy (ToF-SIMS, ION-TOF-SIMS IV) surface analyzer. The surface was cleaned by sputtering 10 keV C_{60}^+ for 2 min. A 25 keV Bi^{3+} primary was used to generate the secondary ions to be analyzed by ToF-SIMS. The Fe K-edge XANES spectra were obtained on the Soft X-ray Microcharacterization Beamline (SXRMB, $\Delta E/E: 10^{-4}$) at the Canadian Light Source (CLS).

Results and discussion

In practical application of lithium-ion batteries, the LiPF_6 -based electrolyte always contains a small amount of water. Also, it is difficult to avoid the moisture contaminations during cell assembly. The existence of even a trace amount of moisture consequently causes the decomposition of the LiPF_6 electrolyte accompanied by the generation of HF, especially at an elevated temperature, as suggested by the following reactions:^{25,26}

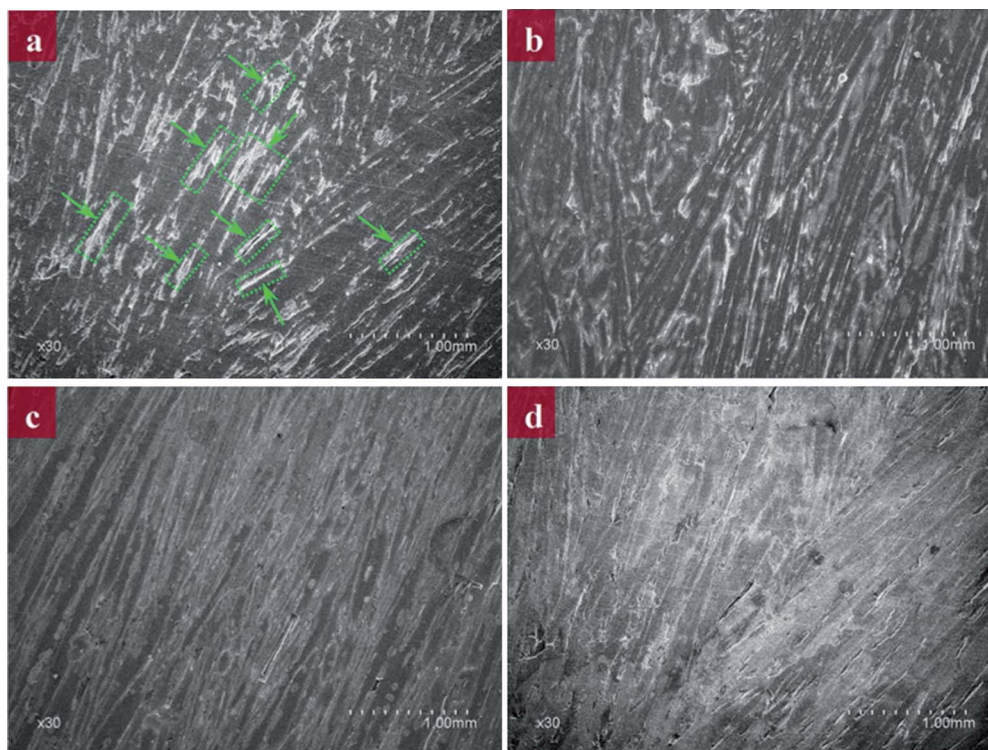
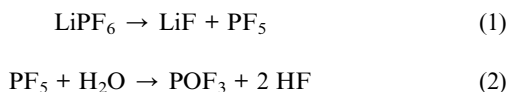


Fig. 1 SEM images of the LiFePO_4 surface during the surface aging process at 0 h (a), 8 h (b), 24 h (c) and 32 h (d).



In our work, 400 ppm H_2O was added to 1 M LiPF_6 solutions to accelerate the surface aging (corrosion) process at room temperature. This water-contaminated electrolyte was therefore considered a corrosive medium because of the accelerated HF generation.

To make it feasible for direct observation of the LiFePO_4 aging process, an ingot material prepared by molten methods was employed, and the surface was polished by sand papers to make it flat and smooth for better observation. Fig. 1 shows surface morphology and the surface corrosion evolution of the polished LiFePO_4 ingot sample stored in moisture-contaminated LiPF_6 . It

is clearly observed that some grain boundaries (bright zone) appear on the fresh LiFePO_4 ingot surface, as shown in Fig. 1a. The formation of these boundaries is related to the metallurgical experiment. Some excess nonstoichiometric reactants with different solidifying temperatures are solidified and separated from LiFePO_4 crystals during cooling of the sample, thus resulting in lots of grain boundaries. The existence of these grain boundaries and the influence on surface chemistry properties of LiFePO_4 was studied in our previous work.²⁷ Here we focus on this bulk LiFePO_4 phase (the flat surface).

After 8 h of storage in H_2O -contaminated LiFePO_4 (Fig. 1b), the surface of the LiFePO_4 sample changed to more rough, and more serious corrosion occurred along the grain boundaries. These boundary sites may also evoke the overall corrosion process during the aging experiment. As shown in Fig. 1c, with a 24 h aging process, more and more corrosion of the surface took

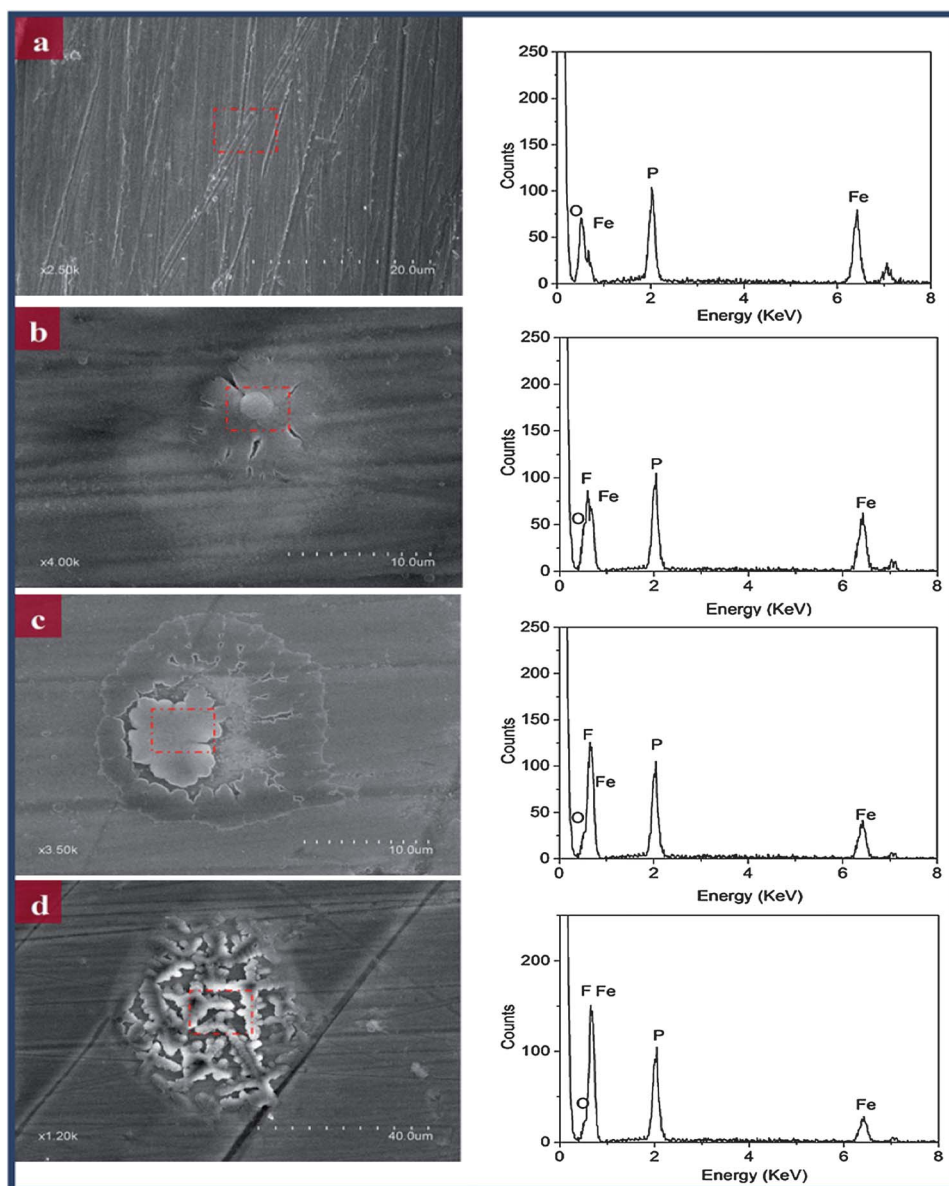


Fig. 2 Iron element dissolves on the LiFePO_4 surface during the surface aging process at 0 h (a), 8 h (b), 24 h (c) and 32 h (d).

place and the corroded zones almost covered the whole surface of LiFePO_4 . After 32 h of the aging process, the surface was completely corroded and became more rough. Moreover, some deeper boundaries were created along the initial boundaries on the surface.

To study and clearly observe the iron dissolution phenomenon, a high resolution SEM study was performed at some typical zones during the aging process. Fig. 2 shows the iron dissolution evolution at some corrosion sites on the LiFePO_4 bulk zone. With the increase of aging time, the LiFePO_4 bulk zone underwent a corrosion process, and the iron element was dissolved gradually at these corrosion sites. EDX indicated that more and more F element appears at these sites. Meanwhile, more and more iron was dissolved from these sites. An element mapping further supports this conclusion. Element mapping at these sites after 8 h and 32 h aging was shown in Fig. 3. Clearly, a large amount of iron was dissolved, which further provides

direct evidence that the corrosion process starts from iron dissolution, which will evoke the overall corrosion process at the LiFePO_4 surface. This corrosion is even worse at some iron-rich impurities on LiFePO_4 , which will be discussed in detail in our future work.

The LiFePO_4 bulk were attacked and reacted directly with HF arising from eqn (1) through the following possible reaction,¹⁵



or



or

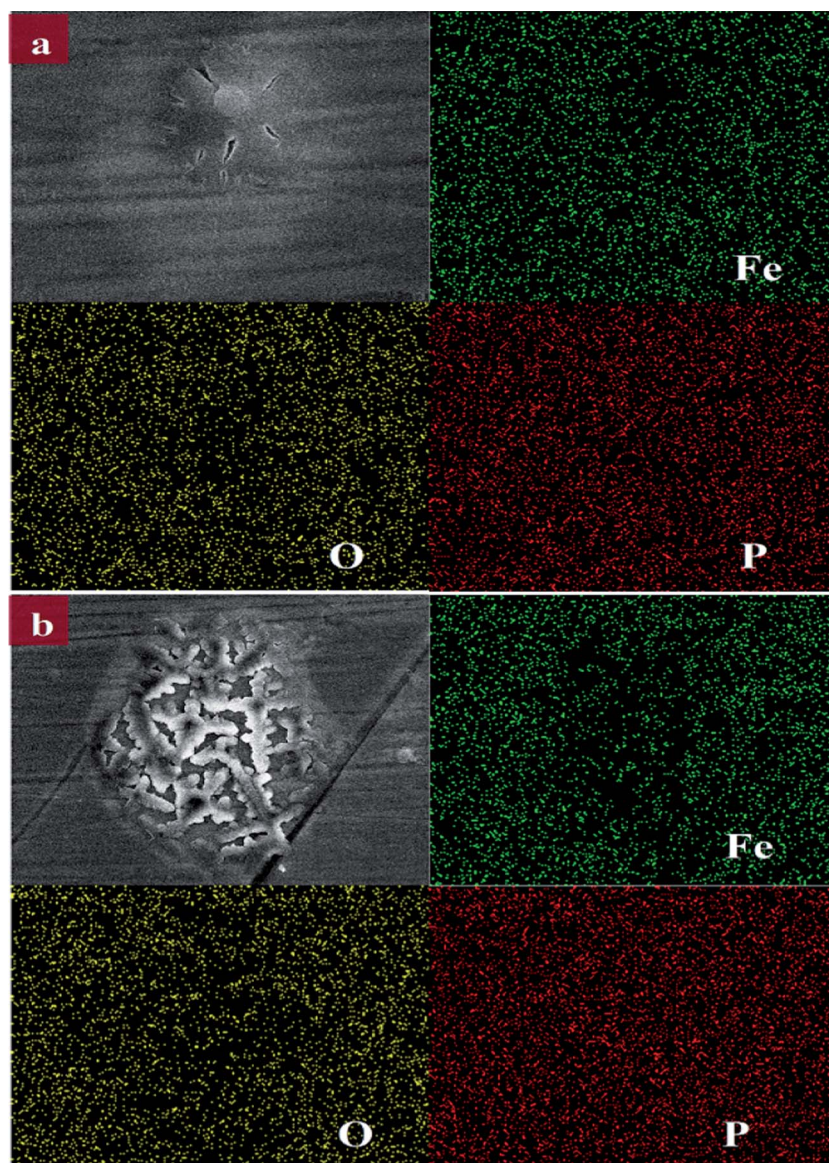


Fig. 3 Element mapping of iron element dissolving during the aging process at 8 h (a) and 32 h (b).

The above study clearly indicates that serious corrosion occurs at LiFePO_4 through Fe dissolution. These undesirable reactions will lead to irreversible changes in the LiFePO_4 structure and the formation of inactive phases, contributing to the capacity fade. In addition, the dissolved iron ions could be reduced to metallic clusters and deposited on negative electrodes. Therefore, a protective layer on LiFePO_4 may be necessary to address these underlying iron dissolution problems by avoiding direct contact of LiFePO_4 with HF.

Surface coating based on metal oxides has proven to be effective for improving the stability of LiFePO_4 because they can act not only as the protection barrier but also the HF scavenger.^{28,29} However, most of metal oxides do not have good electric conductivities. Moreover, the difficulty of uniform coating and high cost also inhibit their practical applications. Thus, an economic and effective surface modification and protection method is more desirable, which evokes us to study the carbon coating protection role in LiFePO_4 stability.

Fig. 4 shows the SEM images of the carbon coated LiFePO_4 . In contrast to the pristine LiFePO_4 (Fig. 1a), the conductivity of C/LiFePO_4 was significantly improved, shown as the brighter image in Fig. 4a, b. A uniform nano-carbon layer was clearly observed in the higher-magnification SEM images (Fig. 4c and d). The carbon layer thickness was determined by FIB combined with HRTEM observation, as shown in Fig. 5. Fig. 5a and b show the slicing and plucking process. A sample with a thickness around 50 nm was obtained for HRTEM analysis. Fig. 5c shows the low-magnification TEM image where a thick Au protection film was clearly observed. There is a narrow line between Au and bulk LiFePO_4 , which is assigned to the carbon coating layer. As shown in high-resolution TEM image in Fig. 5d, the carbon

layer is around 10 nm thick, which may play a protection role in LiFePO_4 .

The same aging experiment in moisture-contaminated LiPF_6 was performed and Fig. 6 shows the SEM images and EDX analysis of C/LiFePO_4 before and after the aging process. After aging, the surface morphology of C/LiFePO_4 showed negligible change, and the corrosion extent is much less than bare LiFePO_4 samples. Although a small amount of the F element was also found at the aged sample, the content was much less than the uncoated LiFePO_4 sample. Furthermore, the iron element exhibited less loss after the aging process. These results clearly indicated that the carbon coating layer significantly reduces the LiFePO_4 surface corrosion rate.

These two aged samples (pristine and carbon coated LiFePO_4) were further characterized by ToF-SMIS, and the magnified ToF-SIMS spectra were shown in Fig. 7. The metal elements were transformed to metal fluoride layers due to HF corrosion during this aging process. For the C/LiFePO_4 sample which shows a strong carbon spectrum, much less of F-containing spectra (F, LiF, and FeF) were found, indicating less degradation of LiFePO_4 by the acidic species during the aging process. By comparison, the pristine LiFePO_4 surface shows much more F-containing spectra due to the bare surface being attacked directly by HF from the electrolyte. It is evident that this carbon coating layer is resistant to HF and further protects LiFePO_4 from HF attack. These results further suggest that the presence of carbon coating provides a protective layer for LiFePO_4 during the aging process.

The changes in the local environment of iron during the aging process were also investigated using Fe K-edge X-ray absorption near-edge structure (XANES) spectra. The energies of

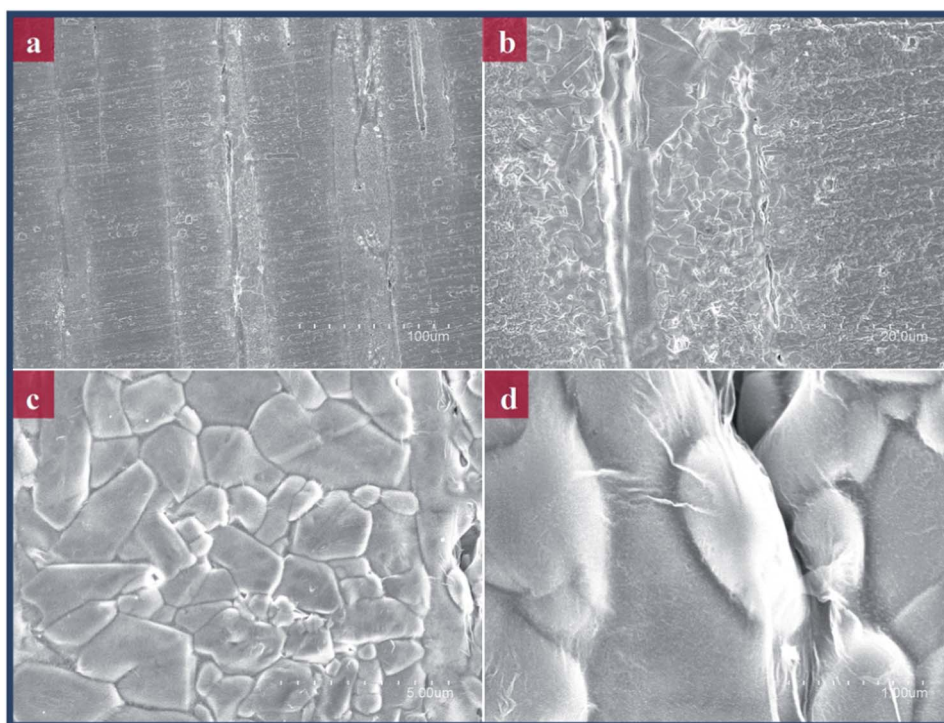


Fig. 4 SEM images of carbon coated LiFePO_4 with different magnifications.

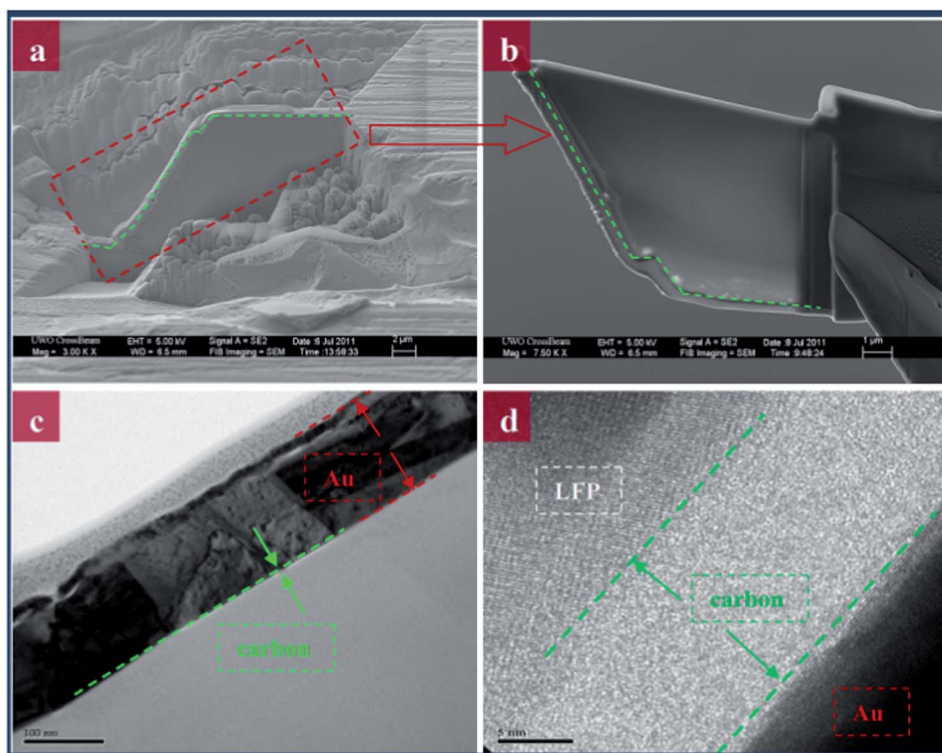


Fig. 5 SEM images of the FIB sample (a and b), TEM (c), and HRTEM (d) images at the carbon layer zone on the FIB sample.

the valence orbital and the edge energy position and the pre-edge features are correlated with the iron chemical valence state in the samples. The result of Fe K-edge XANES for iron ions in the samples are presented in Fig. 8. The edge shift in the spectra indicates the change in the Fe valence state in the samples. The

pristine LiFePO_4 and carbon coated LiFePO_4 show similar spectra, indicating no change in the Fe valence state after carbon coating. However, after the aging process, the positions of Fe K-edge for the two aged samples shift to higher values, indicating a partial oxidation of iron, especially the larger shift

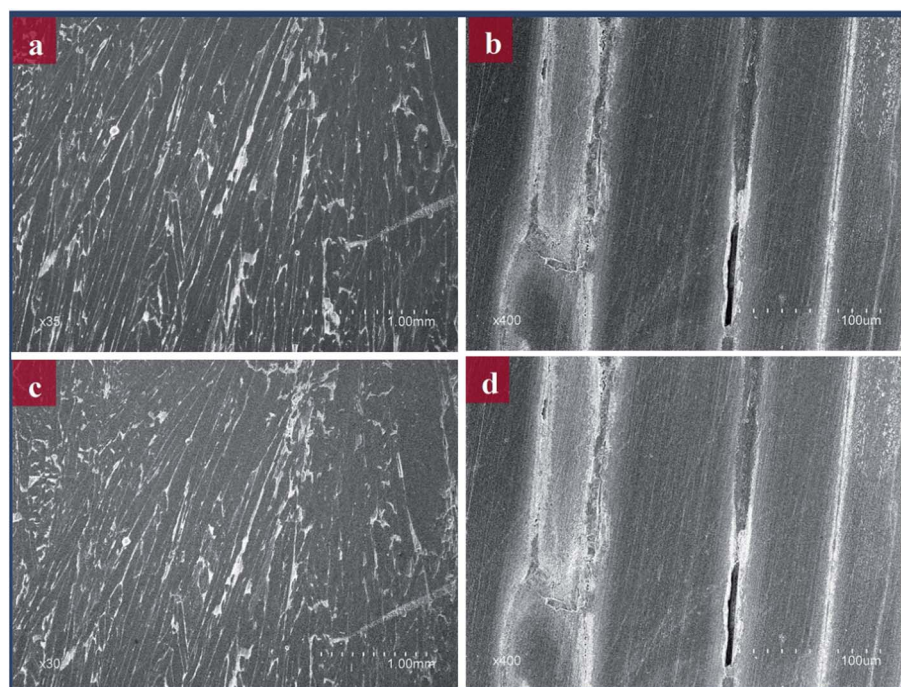


Fig. 6 SEM images of C/LiFePO_4 before (a and b) and after 32 h (c and d) the aging process.

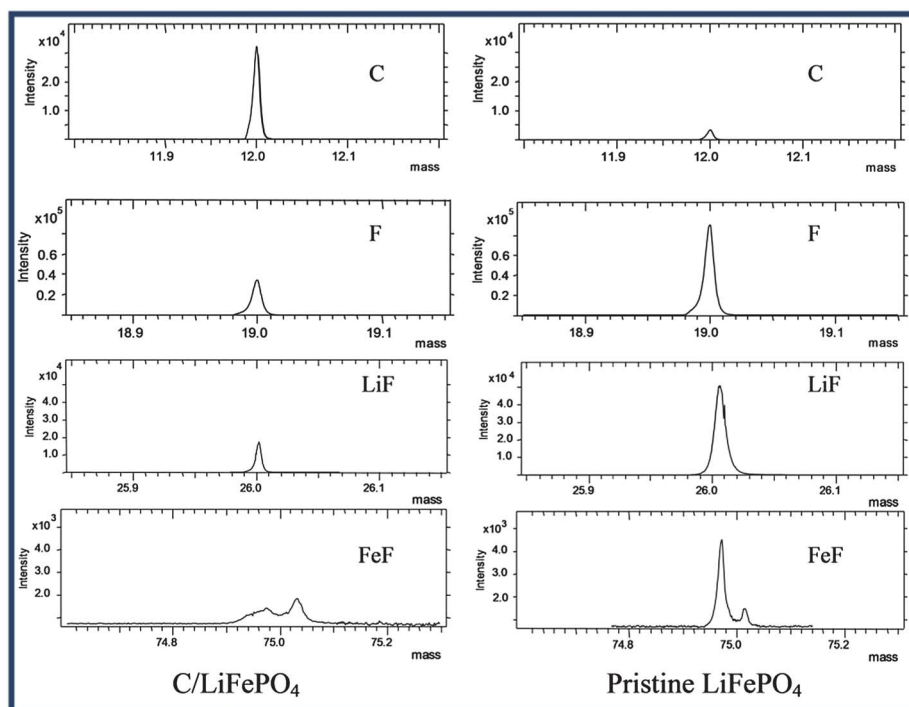


Fig. 7 ToF-SIMS mass spectra of the two aged samples.

was observed at the aged LiFePO_4 sample, indicating more iron oxidation reaction (surface corrosion) occurs at the aged LiFePO_4 without carbon coating layer protection.

A schematic diagram is shown in Fig. 9 to demonstrate the carbon protection role in LiFePO_4 . As confirmed by the above ToF-SIMS, XANES, the surface iron element was corroded, dissolved and transformed to metal fluorides, leading to serious degradation of the LiFePO_4 active material when LiFePO_4 was directly exposed to electrolytes. After carbon coating, the protective carbon layer separates the corrosive medium from LiFePO_4 , protects it from HF attack, and improves the material's stability.

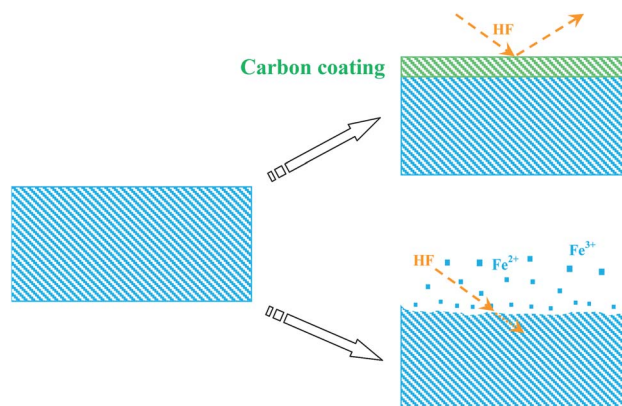


Fig. 9 Schematic diagram of surface corrosion at pristine LiFePO_4 and carbon coated LiFePO_4 .

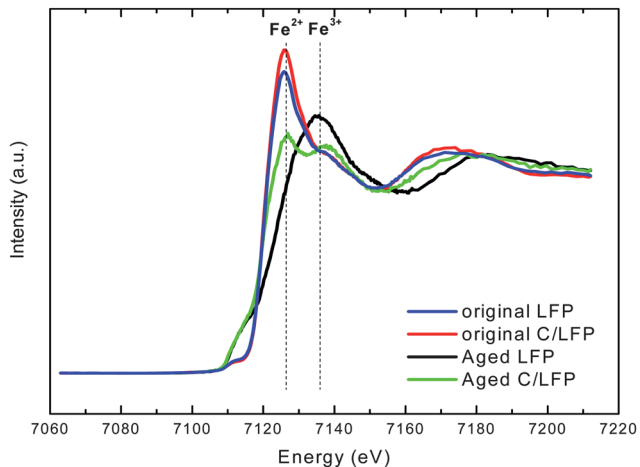


Fig. 8 Fe K-edge XANES spectra of LiFePO_4 samples.

Conclusions

In summary, for the first time, we provided a direct visual observation of the surface corrosion process at olivine LiFePO_4 and direct evidence of iron dissolution evolution. The moisture-contaminated LiPF_6 electrolyte was applied as the corrosion medium due to the presence of HF, which attacks the LiFePO_4 surface and results in iron dissolution. The ingot sample with a flat surface was used as the model material to allow us to observe the surface corrosion process. Further study in carbon coated LiFePO_4 indicated that the carbon coating layer effectively enhances the corrosion resistance through protecting the direct contact with the corrosive medium. Our result provides a deep understanding of the fundamental corrosion process of

LiFePO₄, and indicates that the carbon coating plays a bifunctional role (conductivity improvement and protection barrier) in LiFePO₄. Therefore, applying an effective carbon coating layer, especially ultra-thin coating, is essential for LiFePO₄ and other cathode materials in future better safe batteries.

Notes and references

- 1 A. K. Padhi, K. S. Nanjundaswamy and J. B. Goodenough, *J. Electrochem. Soc.*, 1997, **144**, 1188.
- 2 J. B. Goodenough and Y. Kim, *Chem. Mater.*, 2010, **22**, 587.
- 3 B. L. Ellis, K. T. Lee and L. F. Nazar, *Chem. Mater.*, 2010, **22**, 691.
- 4 A. T. Appapillai, A. N. Mansour, J. Cho and Y. Shao-Horn, *Chem. Mater.*, 2007, **19**, 5748.
- 5 J. Wang and X. Sun, *Energy Environ. Sci.*, 2012, **5**, 5163.
- 6 L. X. Yuan, Z. H. Wang, W. X. Zhang, X. L. Hu, J. T. Chen, Y. H. Huang and J. B. Goodenough, *Energy Environ. Sci.*, 2011, **4**, 269.
- 7 L. Castro, R. Dedryvère, J.-B. Ledeuil, J. Bréger, C. Tessier and D. Gonbeau, *J. Electrochem. Soc.*, 2012, **159**, A357.
- 8 P. Liu, J. Wang, J. Hicks-Garner, E. Sherman, S. Soukiazian, M. Verbrugge, H. Tataria, J. Musser and P. Finamore, *J. Electrochem. Soc.*, 2010, **157**, A499.
- 9 J. Wang, P. Liu, J. Hicks-Garner, E. Sherman, S. Soukiazian, M. Verbrugge, H. Tataria, J. Musser and P. Finamore, *J. Power Sources*, 2011, **196**, 3942.
- 10 M. Dubarry, B. Y. Liaw, M. S. Chen, S. S. Chyan, K. C. Han, W. T. Sie and S. H. Wu, *J. Power Sources*, 2011, **196**, 3420.
- 11 K. Amine, J. Liu and I. Belharouak, *Electrochem. Commun.*, 2005, **7**, 669.
- 12 J.-M. Tarascon, N. Recham, M. Armand, J.-N. Chotard, P. Barpanda, W. Walker and L. Dupont, *Chem. Mater.*, 2010, **22**, 724.
- 13 S.-T. Myung, K. Amine and Y.-K. Sun, *J. Mater. Chem.*, 2010, **20**, 7074.
- 14 Z. Chen, Y. Qin, K. Amine and Y.-K. Sun, *J. Mater. Chem.*, 2010, **20**, 7606.
- 15 M. Koltypin, D. Aurbach, L. Nazar and B. Ellis, *J. Power Sources*, 2007, **174**, 1241.
- 16 Y. Zhang, C.-Y. Wang and X. Tang, *J. Power Sources*, 2011, **196**, 1513.
- 17 H. H. Chang, C. C. Chang, C. Y. Su, H. C. Wu, M. H. Yang and N. L. Wu, *J. Power Sources*, 2008, **185**, 466.
- 18 M. Safaria and C. Delacourt, *J. Electrochem. Soc.*, 2011, **158**, A1123.
- 19 M. Dubarry, B. Y. Liaw, M.-S. Chen, S.-S. Chyan, K.-C. Han, W.-T. Sie and S.-H. Wu, *J. Power Sources*, 2011, **196**, 3420.
- 20 N. Dupré, J.-F. Martin, J. Degryse, V. Fernandez, P. Soudan and D. Guyomard, *J. Power Sources*, 2010, **195**, 7415.
- 21 D. D. McNeil, L. Devigne, C. Michot, I. Rodrigues, G. Liang and M. Gauthier, *J. Electrochem. Soc.*, 2010, **157**, A463.
- 22 M. Gauthier, C. Michot, N. Ravet, J. Dufour, G. Liang, J. Wontcheu, L. Gauthier and D. D. McNeil, *J. Electrochem. Soc.*, 2010, **157**, A453.
- 23 J. Wang, G. Yin, Y. Chen, R. Li and X. Sun, *Int. J. Hydrogen Energy*, 2009, **34**, 8270.
- 24 J. Wang, Y. Chen, Y. Zhang, M. I. Ionescu, R. Li, X. Sun, S. Ye and S. Knights, *J. Mater. Chem.*, 2011, **21**, 18195.
- 25 D. Aurbach, *J. Electrochem. Soc.*, 1989, **136**, 906.
- 26 K. Edström, T. Gustafsson, J. O. Thomas, T. Gustafsson and J. O. Thomas, *Electrochim. Acta*, 2004, **50**, 397.
- 27 J. Wang, J. Yang, Y. Zhang, Y. Li, Y. Tang, M. N. Banis, X. Li, G. Liang, R. Li and X. Sun, *Adv. Funct. Mater.*, 2012, DOI: 10.1002/adfm.201201310.
- 28 Z. Chen, Y. Qin, K. Amine and Y.-K. Sun, *J. Mater. Chem.*, 2010, **20**, 7606.
- 29 I. D. Scott, Y. S. Jung, A. S. Cavanagh, Y. F. An, A. C. Dillon, S. M. George and S. H. Lee, *Nano Lett.*, 2011, **11**, 414.